Manifestations of spatial dispersion in the integral relations in the spectral range of excitonic absorption

S. B. Moskovskii, A. B. Novikov, and L. E. Solov'ev

Yaroslavl State Pedagogical University, 150000 Yaroslavl, Russia and Scientific-Research Institute of Physics, St. Petersburg State University, 198904 St. Petersburg, Russia

(Submitted 18 October 1993)
Zh. Eksp. Teor. Fiz. **105**, 994–1004 (April 1994)

Nonclassical integral effects—temperature dependence of the integral absorption and breakdown of the Kramers–Kronig dispersion relations—observed in the low-temperature transmission spectra of thin crystals near the excitonic absorption lines are attributed to the interference of additional photoexcitonic waves. Expressions are derived for the total absorption coefficient near an isolated excitonic line for two experimental geometries, taking into account the additional waves in the entire spectrum and multiple reflection of light inside the crystal. The results are used for describing experiments performed on thin (up to 0.5 μm thick) plane-parallel CdSe wafers in the temperature range 4–60 K.

1. INTRODUCTION

The role of spatial dispersion (SD) in the optical excitonic reflection and absorption spectra has long been studied[1] (the basic results are reviewed in Chap. V of Ref. 2). Most observed effects are associated with the excitation of additional photoexcitonic waves[1] and are manifested at low temperatures in a narrow spectral range of resonance frequencies of excitonic transitions in perfect single crystals. We show here that effects caused by additional waves are also manifested in the integrated characteristics, to which the entire spectral region of the absorption line contributes.

It is well known that the area under the experimental absorption line contour is determined by the total oscillator strength, and in the usual situation it does not depend on the degree of interaction with the dissipative subsystem (spectral-line broadening is accompanied by a corresponding decrease in absorption at the maximum). In addition, the Kramers–Kronig integral dispersion relations relate uniquely the shape of the absorption contour to the spectral index-of-refraction function.[3,4] We term resonances which exhibit such integral properties classical. The nonclassical behavior of the integral properties in the region of excitonic transitions was manifested experimentally in the breakdown of the Kramers–Kronig relations[5–8] and the temperature dependence of the integral absorption coefficient.[9–11] These effects were predicted qualitatively within the spatial-dispersion theory back in Ref. 1. Among the later theoretical works the temperature dependence of the integral absorption is explained in greatest detail in Ref. 12 on the basis of spatial dispersion. In the process, however, simplifying assumptions are introduced, as a result of which the influence of the additional waves is not taken into account completely, so that the results obtained cannot be used for investigating thin (up to 0.5 μm thick) crystals.

In our previous works[8,13–15] the nonclassical integral effects in excitonic reflection and transmission spectra were explained by the interference of the ordinary and additional waves, which results in the appearance of singularities, associated with the zeros of the amplitude reflection $\rho(\tilde{\omega})$ and transmission $\tau(\tilde{\omega})$ coefficients, in the analytical continuations of the integrands into the upper half-plane of the complex variable $\tilde{\omega}$ (frequency). Elaborating this approach in the present work, we applied it to the description of integral relations for the amplitude-phase transmission spectra of thin plane-parallel CdSe wafers near the $A_{n=1}$ excitonic transition. The investigations were performed for two different light-incidence geometries in a wide temperature range (4–60 K). The angle of incidence was varied for one of the experimental geometries. The experimental results were compared to the theoretical calculations performed using novel formulas for the integral absorption coefficient and the additional term in the Kramers–Kronig dispersion relations. We used these formulas in part in previous work, and in part they are derived here for the first time.

2. THEORY

In the cadmium selenide wafers investigated the $\mathbf{C}_6$ crystal axis was oriented parallel to the surfaces. The geometries in which the transmittance of the plates was studied are displayed in Fig. 1. In the first case (geometry 1) light, polarized in the direction $\mathbf{E} \perp \mathbf{C}_6$, corresponding to polarization of the $A_{n=1}$ dipole excitonic transition in cadmium selenide, was normally incident. In this case, transverse normal photoexcitonic waves, determined by the dispersion relation taking into account spatial dispersion and the boundary conditions on both surfaces, are excited in the crystal. In the second case (geometry 2) light was incident obliquely at different angles φ, and the $\mathbf{C}_6$ axis and the vector $\mathbf{E}$ lay in the plane of incidence. In such a geometry mixed (longitudinal-transverse) normal waves are excited, and the intensity of the photoexcitonic interaction depends on the angle of incidence of the light (the projections of the wave vector on the x and z axes). The form of the permittivity tensor $\varepsilon_{ij}(\omega,\mathbf{k})$, the dispersion equations, and the procedure for solving these equations are well

 1063-7761/94/040533-06$10.00

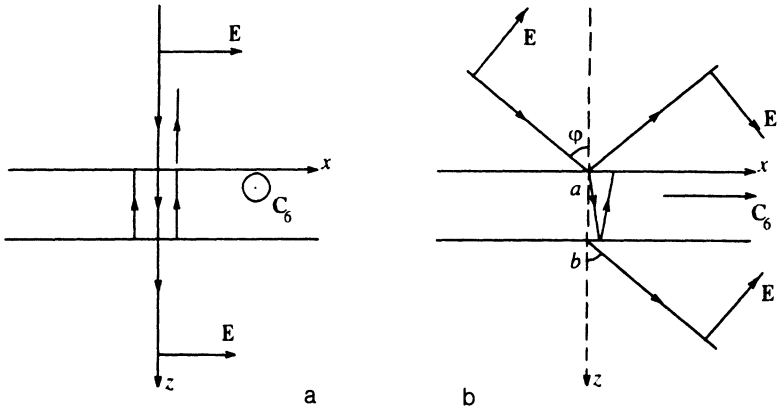

FIG. 1. Experimental geometries: geometry 1 (a) and geometry 2 (b).

known.[16] It is also well known that in determining the dispersion of mixed waves in geometry 2 the tensor character of the effective exciton mass m^* must be taken into account together with the permittivity anisotropy.[17]

The transmittance of the wafers can be described by the amplitude transmission coefficient $\tau(\omega)$, expressing the ratio of the complex amplitudes of the transmitted and incident waves, and the energy transmission coefficients $D(\omega)=\tau(\omega)\tau^*(\omega)$. The absorption is characterized by the spectral function

$$P(\omega)=(1/z)\ln[D_0/D(\omega)],$$

where $D_0=\tau_0\tau_0^*$ is the maximum value of the transmission coefficient in the transmission region and z is the wafer thickness. The spectral changes in the reflection contribute, together with the true absorption, to the values of $\tau(\omega)$, $D(\omega)$, and $P(\omega)$. We are justified, however, in using these functions as the absorption characteristics, since they have the same integral properties as the true absorption spectra and, in addition, they can be compared directly to experiment.

The expression for $\tau(\omega)$ in the geometry 1 was derived in Ref. 18 (see also Chap. IV of Ref. 2), taking into account multiple reflection of light inside the wafer. Pekar's conditions—vanishing of the excitonic contribution to the polarization at the surfaces of the crystal—were used as supplementary boundary conditions (SBCs). We derived the corresponding expression in geometry 2 on the basis of similar assumptions about multiple reflection inside the wafer and Pekar's SBCs. The boundary conditions were written at the points a and b (see Fig. 1), since the phase increments with respect to the point a for different types of waves in the crystal are expressed most symmetrically at the point b, the normal projection of a on the back surface of the wafer. It was found that by introducing appropriate intermediate notation we can put the final expression for the transmission coefficient in geometry 2 into the same form as that obtained in Ref. 18 for transmission in geometry 1:

$$\tau=\frac{2iG}{(1+iF)^2+G^2}. \tag{1}$$

In contrast to the corresponding expression in Ref. 18, the absence of a constant phase factor in Eq. (1) is explained by the choice of origin for the phase of the transmitted wave from the back surface of the wafer (in geometry 2—from the point b), which in our opinion is more convenient. The expressions for the functions G and F in geometries 1 and 2 differ significantly. For geometry 2 they have the form

$$G=\frac{1}{\varepsilon_{0\|}\,(1+q)\cos\varphi}\left[\frac{Q_+}{\sin\delta_+}+q\frac{Q_-}{\sin\delta_-}\right],$$
$$F=\frac{1}{\varepsilon_{0\|}\,(1+q)\cos\varphi}\left[Q_+\operatorname{ctg}\delta_+ + qQ_-\operatorname{ctg}\delta_-\right], \tag{2}$$

where

$$Q_\pm^2=n_\pm^2-\sin^2\varphi,\quad \delta_\pm=\frac{\omega}{c}Q_\pm z,\quad q=\frac{Q_+^2-\varepsilon_1}{\varepsilon_1-Q_-^2},$$

$$n_\pm^2=\varepsilon_1+\sin^2\varphi+\eta\pm\sqrt{\eta^2+\alpha},\quad \varepsilon_1=\varepsilon_{0\|}\left(1-\frac{\sin^2\varphi}{\varepsilon_{0\perp}}\right),$$

$$\eta=\frac{\omega+i\gamma-\omega_L-\beta_\perp\,\varepsilon_1-\beta_\|\,\sin^2\varphi}{2\beta_\perp},\quad \alpha=\frac{\varepsilon_{0\|}\,\omega_{LT}\sin^2\varphi}{\varepsilon_{0\perp}\,\beta_\perp},$$

$n_\pm$ are the complex indices of refraction of normal mixed-type waves; $\varepsilon_{0\|}$ and $\varepsilon_{0\perp}$ are, respectively, the background permittivities for the polarizations $\mathbf{E}\|\,\mathbf{C}_6$ and $\mathbf{E}\perp\mathbf{C}_6$;

$$\beta_\|=\frac{\hbar\omega^2}{2m_\|^*c^2},\quad \beta_\perp=\frac{\hbar\omega^2}{2m_\perp^*c^2},$$

$m_\|^*$ and $m_\perp^*$ are, respectively, the effective masses of excitons with wave vectors $\mathbf{k}\|\,\mathbf{C}_6$ and $\mathbf{k}\perp\mathbf{C}_6$; ω_L and ω_{LT} are, respectively, the frequency of the longitudinal exciton and the frequency of the longitudinal-transverse splitting in the limit $\mathbf{k}\to 0$; c is the speed of light in free space; and γ is the damping constant. Expressions for G and F, which must employed in Eq. (1) in order to calculate the transmission in geometry 1, are presented in Ref. 18.

The integral absorption coefficient in the approximation of an isolated resonance is calculated from the formula

$$S=\frac{1}{z}\int_{-\infty}^{\infty}\ln\frac{D_0}{D(\nu)}\,d\nu, \tag{3}$$

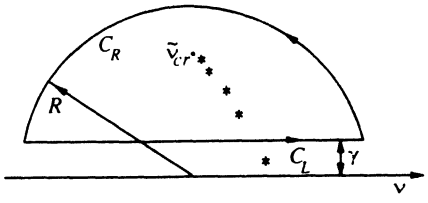

FIG. 2. Integration contour in the upper half-plane of the complex frequency.

which can be easily put into the form

$$S=\frac{2}{z}\,\mathrm{Re}\int_{-\infty}^{\infty}\frac{\nu}{\tau}\frac{d\tau}{d\nu}\,d\nu, \tag{4}$$

where ν is the spectral variable, measured in cm^{-1}.

Consider the integral

$$I=\int_C \frac{(\tilde{\nu}-i\gamma)}{\tau(\tilde{\nu})}\frac{d\tau(\tilde{\nu})}{d\tilde{\nu}}\,d\tilde{\nu}, \tag{5}$$

where $\tilde{\nu}$ is the complex spectral variable, $\tau(\tilde{\nu})$ is the analytical continuation of the function $\tau(\nu)$; and the integration contour C consists of a rectilinear section C_L, determined by the equation $\mathrm{Im}\,\tilde{\nu}=\gamma$, and a semicircle C_R of radius R centered on the real axis (Fig. 2). The integral in Eq. (5) can be written as the sum $I=I_L+I_R$ in accordance with the partitioning of the integration contour. Then, passing to the limit $R\to\infty$ we obtain the following expression for the desired integral (4):

$$S=\frac{2}{z}\,\mathrm{Re}\,I_L=\frac{2}{z}\,\mathrm{Re}(I-I_R). \tag{6}$$

As shown in Ref. 8, the complex amplitude reflection and transmission coefficients are, by definition, the local response functions of the medium (including, even when spatial dispersion is taken into account). It is well known that due to the causality principle such functions have an analytic continuation with no singular points in the upper half-plane of the complex variable $\tilde{\nu}$.[3,4] Thus inside the integration contour the only singularities of the integrand in Eq. (5) are poles corresponding to the zeros of the function $\tau(\tilde{\nu})$. As mentioned above, when the spatial dispersion is taken into account zeros of the transmission become possible as a result of interference between the ordinary and additional waves. We have developed a numerical method for solving the equation $\tau(\tilde{\nu})=0$ for different light-incidence geometries. The coordinates ν_{0j} and γ_{0j} of the transmission zeros and the number of zeros depend on the thickness of the crystal, and in geometry 2 they also depend on the angle of incidence. The zero points lie along the curve [in the upper half-plane of the variable $\tilde{\nu}$ (see Fig. 2)] which is the bottom of the valley of the function $|\tau(\nu,\gamma)|$, described approximately by the condition $\mathrm{Im}\,n_+=\mathrm{Im}\,n_-$. As the thickness of the crystal increases, the zero points move in the direction of the critical point $\tilde{\nu}_{cr}$, corresponding to the condition $n_+(\tilde{\nu})=n_-(\tilde{\nu})$, and new zeros appear in the region adjoining the real axis. The position of the point $\tilde{\nu}_{cr}$ in the geometry 2 depends on the angle of incidence of the light.

Once the coordinates of the zero points of the function $\tau(\tilde{\nu})$ are known, the integral (5) can be calculated:

$$I=2\pi i\sum_j[\nu_{0j}+i(\gamma_{0j}-\gamma)]. \tag{7}$$

The summation in Eq. (7) extends only over the zeros in the region bounded by the contour C, i.e., points with $\gamma_{0j}>\gamma$, so that for $\gamma>\gamma_{cr}=\mathrm{Im}\,\tilde{\nu}_{cr}$ the integral (5) vanishes. In order to calculate the integral I_R it is convenient to switch to the dimensionless complex spectral variable η and place the center of the semicircle C_R at the point corresponding to $\eta=0$. The integrand in Eq. (5) can be expanded in a series in powers of $(1/\eta)$, the series containing terms of first and higher integer and half-integer orders. In the integration over C_R only the first-order term makes a nonvanishing contribution to I_R in the limit $R\to\infty$ ($|\eta|\to\infty$). Substituting the result of the integration into Eq. (6) we obtain finally

$$S=S_0-\frac{4\pi}{z}\sum_j(\gamma_{0j}-\gamma), \tag{8}$$

where S_0 is the contribution from integration over C_R. It depends on the parameters of the excitonic transition, the thickness of the wafer, and the angle of incidence (in the geometry 2), being independent of the damping constant. The second term represents the contribution of the transmission interference zeros, lying in the region bounded by the contour C. Calculating S_0 in geometry 1 gives

$$S_0=\pi\nu_{LT}k_0\times\frac{(1+R_0)/(1-R_0)+\sqrt{F_0}\sin(2k_0z)/2k_0z}{1+F_0\sin^2(k_0z)}, \tag{9}$$

where

$$k_0=\frac{2\pi}{\lambda_T}\sqrt{\varepsilon_{0\perp}},\quad R_0=\left(\frac{1-\sqrt{\varepsilon_{0\perp}}}{1+\sqrt{\varepsilon_{0\perp}}}\right)^2$$

are, respectively, the wave vector and the reflectivity of the crystal surface, and in the polarization considered they correspond to the background permittivity near the wavelength λ_T of the transverse exciton; the parameter F_0 is given by

$$F_0=\frac{4R_0}{(1-R_0)^2}=\frac{(\varepsilon_{0\perp}-1)^2}{4\varepsilon_{0\perp}}.$$

In the geometry 2 we have

$$S_0=\pi\nu_{LT}k_{0z}\frac{\sin^2\varphi}{\varepsilon_{0\perp}-\sin^2\varphi}\times\frac{(1+R_1)/(1-R_1)+\sqrt{F_1}\sin(2k_{0z}z)/2k_{0z}z}{1+F_1\sin^2(k_{0z}z)}, \tag{10}$$

where $k_{0z}=2\pi/\lambda_T\sqrt{\varepsilon_1}$ and $R_1=(1-\sqrt{\varepsilon_2}/1+\sqrt{\varepsilon_2})^2$ are, respectively, the normal component of the wave vector and

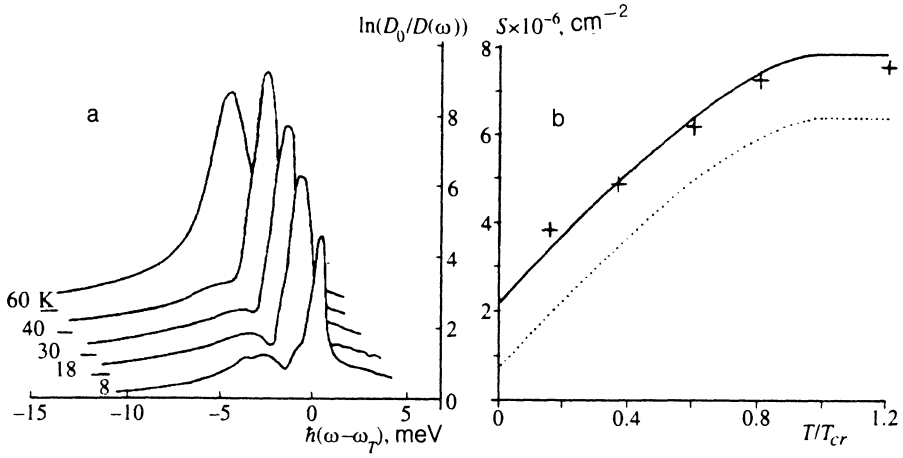

FIG. 3. (a) Experimental absorption contours in geometry 1 at different temperatures (the frequency is measured from the value of ω_T at $T=8$ K); (b) temperature dependence of the integral absorption: the solid curve was computed using Eqs. (8)–(9); the dashed line was computed using similar equations neglecting multiple reflections in the crystal; the marks are the experimental values of S.

the reflectivity of the crystal surface, which correspond to the background permittivities in the resonance region,

$$\varepsilon_2=\varepsilon_1/(\varepsilon_{0\|}\cos\varphi)^2, \quad F_1=\frac{4R_1}{(1-R_1)^2}=\frac{(\varepsilon_2-1)^2}{4\varepsilon_2}.$$

In the geometry 1 the absorption line is completely polarized. This allows the phase spectrum in the absorption region to be recorded by methods based on the interference of polarized waves, using as the reference signal the transmitted wave in the polarization corresponding to no absorption. Combined amplitude-phase measurements in transmission open up the possibility of using augmented dispersion relations.[8] The relation which makes it possible to retrieve the phase function from the transmission spectrum has the form

$$\delta(\nu)=\frac{\nu}{\pi}\int_0^\infty \frac{\ln[D_0/D(x)]}{x^2-\nu^2}\,dx + \sum_j\left[2\ \mathrm{arctg}\frac{\gamma_{0j}-\gamma}{\nu_{0j}-\nu}+a_j\right], \qquad (11)$$

where $a_j=0$ for $\nu<\nu_{0j}$ and $a_j=2\pi$ for $\nu\geqslant\nu_{0j}$. Just as in Eq. (7), only terms with $\gamma_{0j}>\gamma$ are included in the sum. For $T>T_{cr}$ the nonintegral term thus vanishes, and Eq. (11) becomes the classical Kramers–Kronig dispersion relation. It is important to note that the manifestation of spatial dispersion in the temperature dependence of the integral absorption and in the integral dispersion relations is studied from a unified point of view, and it depends on the same parameters—the coordinates of the transmission zeros in the upper half-plane of the complex frequency.

3. DESCRIPTION OF THE EXPERIMENT AND RESULTS

The experiments were performed on thin ($\sim$0.4 μm thick) plane-parallel CdSe wafers. The samples were prepared and installed so that no stresses arose with decreasing temperature. In order to reduce the influence of nonuniformities in the sample, the irradiated zone was limited to dimensions of 0.1×0.1 cm^2. The crystals were placed into a liquid-helium cryostat, in which a temperature-stabilized volume was created with the help of a heater and temperature sensor. When the spectrum was recorded, the temperature of the sample was maintained constant to within 0.1 K. The light transmitted through the crystal was analyzed with a DFS-24 spectrometer (linear dispersion 4 Å/mm) and recorded using a photon-counting scheme. A microcomputer synchronized the operation of the apparatus. The microcomputer also controlled a stepping motor, which performed the scanning; it accepted and stored data fed into it from the recording system; and it monitored the constancy of the temperature of the sample. A signal recorded in parallel was displayed on an oscillograph and recorded with an X–Y recorder. The program that performed mathematical processing of the signal assumed that the spectrum was normalized to the transmission far from resonance (in the transmission range) and that the spectral distribution of the energy of the light source and the dark current of the photomultiplier were taken into account. In addition, the contribution of the $A_{n=2}$ exciton and other higher-order states on the short-wavelength side of the absorption line studied was subtracted out. The spectral dependence of this contribution was described by a parabola, which was determined according to three reference points, similarly to the method described in Ref. 19.

The experimental absorption spectra in geometry 1 for a 0.37 μm thick crystal wafer in the temperature range 8–60 K are displayed in Fig. 3a. When the temperature increases up to the temperature of critical damping, the absorption at the maximum increases, as is typical of spatial dispersion. With further heating the temperature dependence of the absorption contour becomes classical. The critical temperature for the given sample is about 50 K. The experimental values of the integral absorption, which was obtained by numerically integrating the spectra using Eq. (3), are compared in Fig. 3b to the theoretical curves calculated from Eqs. (8)–(9). The temperature dependence of the damping constant was assumed to be monotonic. It was also assumed that the impurities and defects make a constant contribution to the damping, and that the contribution of scattering by phonons grows linearly with the temperature.[20] The figure also displays the computed temperature dependence of the integral absorption neglecting multiple reflections of light in the crystal.[14] The calculations based on Eqs. (8)–(9) agree much better with the experimental data.

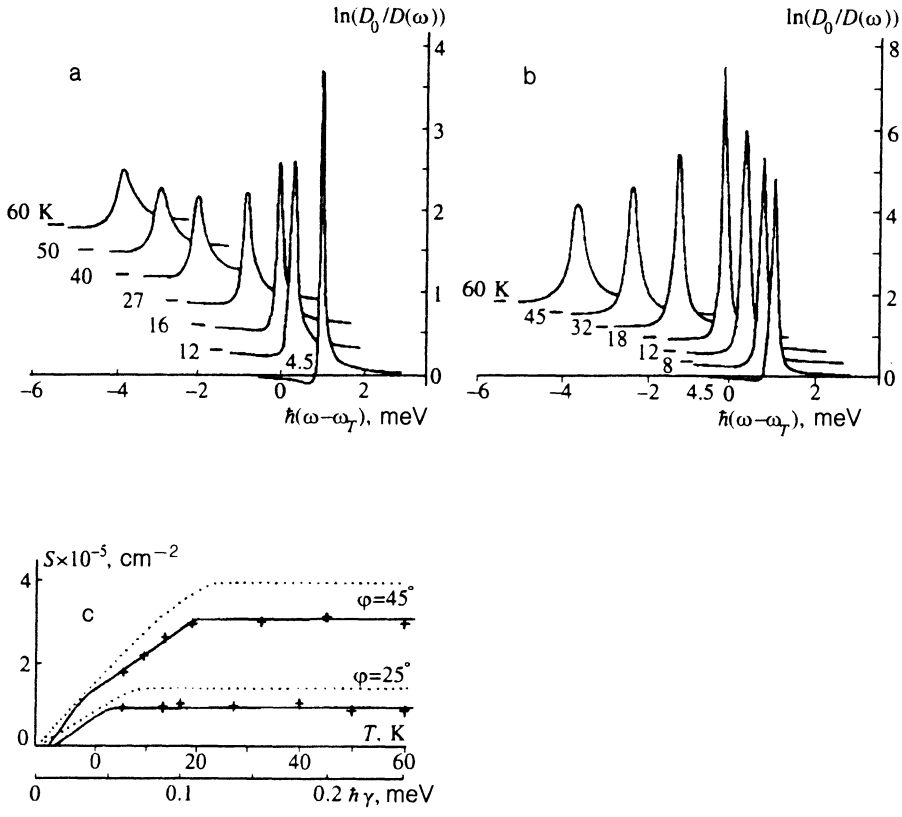

FIG. 4. Experimental absorption contours in geometry 2 with incidence angles $\varphi=25°$ (a) and $\varphi=45°$ (b) and different temperatures (the frequency is measured from the value of ω_T at $T=4.5$ K); (c) integral absorption versus the temperature and damping constant: the solid curves were computed using Eqs. (8) and (10); the dashed curve was computed by a method similar to Ref. 12; the crosses are the experimental values of S.

The absorption spectra in geometry 2 for two angles of incidence of light in the temperature range 4.5–60 K are presented in Fig. 4a ($\varphi=25°$) and Fig. 4b ($\varphi=45°$). The spectra were obtained for the same 0.41 μm thick sample. For angle of incidence $\varphi=25°$ the temperature dependence of the absorption line contour is classical, while for $\varphi=45°$ up to $T=18$ K the absorption at maximum and the area under the contour are observed to increase. At higher temperatures the area under the absorption curve no longer changes, and a decrease in absorption at maximum is accompanied by broadening of the line. This behavior of the absorption spectra indicates that the critical temperature is less than 4.5 K for $\varphi=25°$ and $T_{cr}\approx 18$ K for $\varphi=45°$; this agrees with the theoretical notions about the dispersion of a mixed exciton for which $\gamma_{cr}\sim\sin\varphi$. Figure 4c displays the temperature dependence of the integral absorption coefficient. The damping scale was converted into the temperature scale by the method described above using four values of S with $\gamma<\gamma_{cr}$ for $\varphi=45°$. For comparison, the curves computed by a method similar to Ref. 12 and employed by us previously in Ref. 13 for the mixed-exciton geometry are also displayed in the figures.

The phase spectra were recorded with an automatic apparatus, controlled by the microcomputer. A quartz wedge was used in order to introduce an additional phase difference between polarizations parallel and perpendicular to $\mathbf{C_6}$ into the incident light wave, polarized at an angle of 45° with respect to the $\mathbf{C_6}$ axis of the wafer. This additional phase difference was modulated with an acoustic frequency by oscillating the wedge. As the spectrum was scanned, the signals at the fundamental and doubled modulation frequency, which were proportional to $U_1\sim\sin\delta$ and $U_2\sim\cos\delta$, were recorded separately. Adjusting the modulation amplitude can then equalize the coefficients of proportionality. Then

$$\delta(\nu)=\text{arctg}^{-1}(U_1/U_2).$$

The experimental phase spectra for a 0.37 μm thick sample are compared in Fig. 5 to the transmission spectra computed with the help of the relation (11) for the temperatures $T=8$ K (a) and $T=60$ K (b). The high-temperature-phase spectrum is described, to a high degree of accuracy, by the classical integral term in Eq. (11). At $T=8$ K the curve calculated using the classical Kramers–Kronig relation disagrees, both quantitatively and qualitatively, with the experiment (in the figure the scale along the vertical axis for this curve is magnified by a factor of four), while the curve calculated using Eq. (11), taking into account the contribution of the transmission zeroes, agrees well with experiment. The value of the damping constant employed for calculating the phase using Eq. (11) was chosen so that the calculation would agree with experiment, taking into account the value of the total absorption. Similar measurements and calculations were performed for other temperatures. This gave the following damping coefficients:

T, K	8	18	30	40
$\hbar\gamma$, meV	0.10±0.02	0.15±0.02	0.23±0.02	0.30±0.02

We note that the values obtained, using Eq. (8), for the damping at $T<T_{cr}$ from the measurements of the total absorption and from combined amplitude-phase measurements, using Eq. (11), agree to within the limits of error,

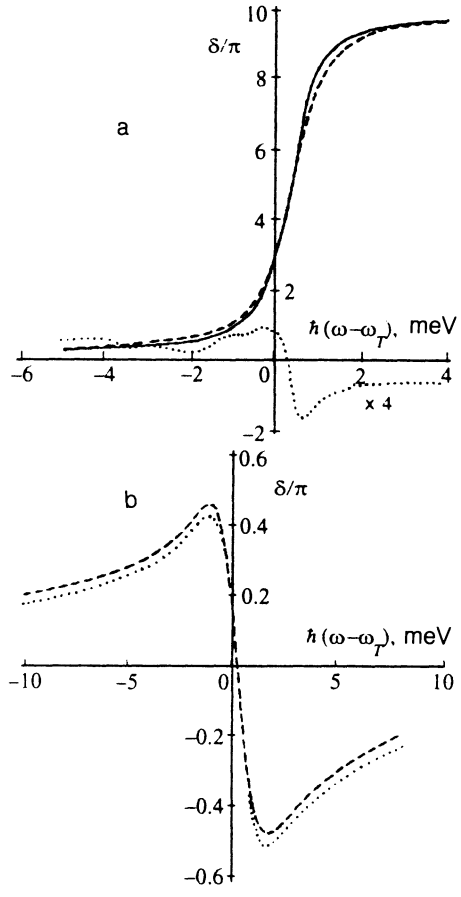

FIG. 5. Comparison of the experimental transmission phase spectra in geometry 1 to the phase spectra computed with the help of the dispersion relations from the absorption spectra at temperatures 8 K (a) and 60 K (b): the solid curve was computed using Eq. (11); the dashed curves represent the experimental values; and, the dotted curves were computed using the classical Kramer–Kronig relations.

and they agree with the assumptions made above concerning the character of the temperature dependence $\gamma(T)$. In constructing the plots $S(T)$ (Figs. 3 and 4) we also extrapolated these assumptions into the temperature range $T > T_{cr}$. However, other data (the width of the contour and the magnitude of the absorption at maximum) indicate that the damping increases more rapidly with temperature at temperatures $T > T_{cr}$.

[1] S. I. Pekar, Zh. Eksp. Teor. Fiz. **33**, 1022 (1957) [Sov. Phys. JETP **6**, 785 (1957)].
[2] S. I. Pekar, *Crystal Optics and Additional Light Waves*, Benjamin, Reading, MA, 1983.
[3] L. D. Landau and E. M. Lifshitz, *Electrodynamics of Continuous Media*, Pergamon Press, N. Y., 1983.
[4] H. M. Nussenzveig, *Causality and Dispersion Relations*, Academic Press, N. Y., 1972.
[5] M. S. Brodin, A. F. Prikhot'ko, and M. S. Soskin, Opt. Spektrosk. **6**, 28 (1959).
[6] M. S. Brodin and M. I. Strashnikova, Fiz. Tverd. Tela **4**, 2454 (1962) [Sov. Phys. Solid State **4**, 1798 (1963)].
[7] I. Filinski and T. Skettrup, Solid State Commun. **11**, 1651 (1972).
[8] S. B. Moskovskii and L. E. Solov'ev, Zh. Eksp. Teor. Fiz. **86**, 1419 (1984) [Sov. Phys. JETP **59**, 831 (1984)].
[9] J. Voigt, Phys. Status Solidi B **64**, 549 (1974).
[10] F. I. Kreingol'd and V. L. Makarov, Pis'ma Zh. Eksp. Teor. Fiz. **20**, 441 (1974) [JETP Lett. **20**, 201 (1974)].
[11] A. B. Novikov, L. E. Solov'ev, and V. G. Talalaev, Fiz. Tverd. Tela **28**, 1931 (1986) [Sov. Phys. Solid State **28**, 1079 (1986)].
[12] N. N. Akhmediev, Zh. Eksp. Teor. Fiz. **79**, 1534 (1980) [Sov. Phys. JETP **52**, 773 (1980)].
[13] S. R. Grigor'ev, S. B. Moskovskii, A. B. Novikov, and L. E. Solov'ev, Vestnik LGU, Ser. 4, 107 (1987).
[14] S. B. Moskovskii, A. B. Novikov, and L. E. Solov'ev, Fiz. Tverd. Tela **30**, 1431 (1988) [Sov. Phys. Solid State **30**, 826 (1988)].
[15] S. B. Moskovskii, A. B. Novikov, O. S. Omegov, and L. E. Solov'ev, Fiz. Tverd. Tela **33**, 657 (1991) [Sov. Phys. Solid State **33**, 375 (1991)].
[16] V. M. Agranovich and V. L. Ginzburg, *Crystal Optics with Spatial Dispersion and Excitons*, Springer-Verlag, N.Y., 1984.
[17] S. A. Permogorov, A. V. Sel'kin, and V. V. Travnikov, Fiz. Tverd. Tela **15**, 1822 (1973) [Sov. Phys. Solid State **15**, 1215 (1973)].
[18] S. I. Pekar, Zh. Eksp. Teor. Fiz. **34**, 1176 (1958) [Sov. Phys. JETP **7**, 813 (1958)].
[19] A. B. Pevtsov, S. A. Permogorov, and A. V. Sel'kin, Pis'ma Zh. Eksp. Teor. Fiz. **39**, 261 (1984) [JETP Lett. **39**, 312 (1984)].
[20] A. A. Demidenko, Fiz. Tverd. Tela **5**, 489 (1963) [Sov. Phys. Solid State **5**, 357 (1963)]; Fiz. Tverd. Tela **5**, 2835 (1963) [Sov. Phys. Solid State **5**, 2074 (1963)].

Translated by M. E. Alferieff